IJECEC INTERNATIONAL JOURNAL OF ELECTRICAL AND COMPUTER COMMUNICATION ENGINEERING
ISSN(Online):2533-8945
VOLUME 4 ISSUE 4

SVPWM BASED COMPREHENSIVE ANALYSIS AND REDUCTION OF TORQUE RIPPLES IN THREE-PHASE FOUR-SWITCH INVERTER-FED PMSM

[#1]MATTA RAVI TEJA, PG STUDENT
[#2]A.RAMAKRISHNA, ASSISTANT PROFESSOR
[#3]Dr.J.V.G RAMA RAO, PHD, PROFESSOR
DEPARTMENT OF EEE
BONAM VENKATA CHALAMAYYA ENGINEERING COLLEGE

ABSTRACT: As a result of their reduced number of switches, three-phase four-switch (TPFS) inverters are generally applied as cost-reduction topologies for permanent magnet synchronous motor (PMSM) drives. However, the torque ripples of PMSMs severely deteriorate the performance and reliability of the entire system. Hence, comprehensive considerations for torque ripple reduction, including high- and low-frequency torque ripples, are elaborated considering TPFS inverter-fed PMSM drives. The second-order torque harmonics produced by DC capacitor voltage fluctuations are first demonstrated, and a very simple compensation method is prese nted by introducing a novel non-orthogonal coordinate transformation. Then, to evaluate the effects on the high-frequency torque ripples of space vector modulation (SVM) schemes, three SVM schemes for TPFS inverter-fed PMSM drives are assessed based on the torque ripple root mean square (RMS) value. Consequently, the preferred SVM scheme is obtained for high-frequency torque ripple minimization. Moreover, the linear modulation range of the TPFS inverter-fed PMSM drive is derived considering capacitor voltage fluctuations, therein avoiding the low-frequency torque ripples caused by over-modulation. Meanwhile, an adaptive capacitor voltage offset suppression method is proposed to fully exploit the DC link voltage. The experimental results demonstrate the validation and effectiveness of the proposed analysis and methods for torque ripple reduction.

Index Terms—Capacitor voltage fluctuation, permanent magnet synchronous motor (PMSM) drives, space vector modulation (SVM), three-phase four-switch (TPFS) inverter, torque ripple reduction

I.INTRODUCTION

PERMANENT magnet synchronous motors (PMSMs), driven by three-phase voltage-source inverters with six switches (TPSS), have become the central aspect of variable-frequency drive systems in many industrial applications because of their superior features such as their high efficiency and high power density. However, in certain applications, cost reduction of the inverter configuration is taken as the priority. Therefore, the three-phase four-switch (TPFS) inverter presented in [1]-[11] represents a promising option for replacing the TPSS inverters due to its reduced number of power switches. In addition, the TPFS inverter can be utilized to ride through open/short-circuit faults of the TPSS inverter, which is quite valuable in some critical applications, such as wind power generation [7], [8].

In PMSM drives, an inherent drawback to be inhibited is torque ripples, which cause undesirable acoustic noise and torsional vibrations, even resulting in shaft failures [12], [13]. Hence, several techniques for the torque ripple reduction are introduced to improve the performance of PMSM drives. In [14]-[17], the cogging torque of a PMSM is suppressed using motor design techniques such as skewing, fractional slot pitch winding and optimized magnetic design. In [18]-[24], the pulsating torque caused by the back-EMF harmonics in the PMSM is compensated by active control methods, such as repetitive control, iterative learning control and self-adaptive control. Furthermore, as a prominent consequence of the nonsinusoidal voltages impressed by the converters, the high frequency torque harmonics in PMSMs are strongly influenced by the adopted voltage vectors during the switching period [12], [13]. Therefore, [25]-[29] utilize additional active vectors and optimize their duration times during the switching period to reduce torque ripples in direct-torque-controlled (DTC) PMSM drives. However, torque ripple reduction methods are mainly focused on TPSS inverter-fed PMSM drives. Still, some other considerations for torque ripples remain to be applied to TPFS inverter-fed PMSM drives. In TPSS inverter-fed PMSM drives, the neutral point voltage of the DC bus is constant, which has no effect on the torque performance. In contrast, in a TPFS inverter-fed PMSM drive, one phase of stator current

ISSN(Online):2533-8945
VOLUME 4 ISSUE 4

directly flows into the midpoint of the DC split capacitors, resulting in periodical fluctuations of the capacitor voltages. However, the modulation techniques for TPFS inverters discussed in [1]-[11] ignore the capacitor voltage oscillations; thus, imbalanced stator currents are produced, resulting in pulsating torques. Moreover, due to the absence of zero vectors in the TPFS inverter, various equivalent zero vector synthesis approaches in the space vector modulation (SVM) are proposed in [1]-[11]. However, the effects on the high frequency torque harmonics of the zero vector synthesis methods have not been analyzed in detail.

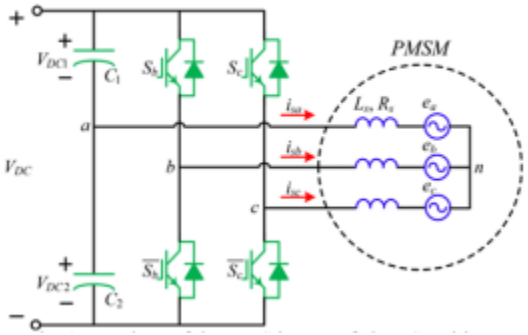

Fig. 1. Topology of the TPFS inverter-fed PMSM drive.

Therefore, an in-depth analysis of torque ripples influenced by the SVM strategies in a TPFS inverter-fed PMSM drive for reducing the high-frequency torque harmonics should be provided. In addition, the capacitor voltage fluctuations strongly impact the linear modulation range of the TPFS inverter, which has not been mentioned previously. If the capacitor voltage fluctuations are not considered, the TPFS inverter-fed PMSM drive may operate in the over-modulation zone with an improper DC bus voltage, thus producing abundant low-frequency torque harmonics. Meanwhile, the linear modulation range also deteriorates as a result of the DC offset of the two capacitor voltages, which should be eliminated. However, the capacitor voltage offset suppression method in [6] and [7] utilizes a second-order low pass filter (LPF) to extract the DC offset component, which is not applicable to TPFS inverter-fed PMSM drives under low-speed conditions due to the reduced stability margin of the control loop caused by the limited bandwidth of the LPF. Thus, an improved capacitor voltage offset suppression method applicable to TPFS inverter-fed PMSM drives is required to eliminate the low-frequency torque ripple caused by the limited linear modulation range.

In this study, the comprehensive analysis of torque ripple reduction is presented in terms of a TPFS inverter-fed PMSM drive, including the modulation scheme, the linear modulation range, and a suitable control strategy. The pulsating torque in the TPFS inverter-fed PMSM drive produced by the uncompensated modulation strategies is first illustrated, and a simple compensated method is proposed to directly obtain the duty ratios by introducing a novel coordinate transformation. Then, the influence on the high-frequency torque harmonics of the SVM strategies is analyzed by introducing the root mean square (RMS) value of the torque ripple. Additionally, three SVM strategies for TPFS inverter-fed PMSM drives are analytically evaluated in terms of their abilities to reduce the high-frequency torque ripples. Moreover, the linear modulation range of the TPFS inverter-fed PMSM drive is fully investigated considering capacitor voltage fluctuations. According to the proposed analysis, appropriate DC bus voltages under various operating conditions can be easily obtained to eliminate the low frequency torque ripple caused by over-modulation. Meanwhile, an adaptive DC offset voltage suppression method that is suitable for TPFS inverter-fed PMSM drives under any operating condition is proposed. Consequently, the DC bus voltage is fully exploited to eliminate the low-frequency torque ripple caused by the capacitor voltage offset. The simultion results show that the proposed analysis and methods for torque ripple reduction are valid and effective.

II. SPACE VECTOR MODULATION

Space vector modulation (**SVM**) is an algorithm for the control of pulse width modulation (PWM).[1] It is used for the creation of alternating current (AC) waveforms; most commonly to drive 3 phase AC powered motors at varying speeds from DC using multiple class-D amplifiers. There are variations of SVM that result in different quality and computational requirements. One active area of development is in the reduction of total harmonic distortion (THD) created by the rapid switching inherent to these algorithms.

IJECEC INTERNATIONAL JOURNAL OF ELECTRICAL AND COMPUTER COMMUNICATION ENGINEERING
ISSN(Online):2533-8945
VOLUME 4 ISSUE 4

Principle:

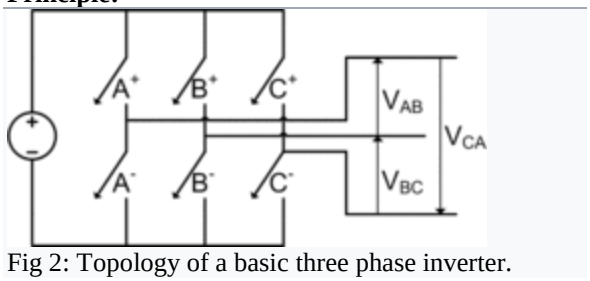

Fig 2: Topology of a basic three phase inverter.

A three-phase inverter as shown to the right converts a DC supply, via a series of switches, to three output legs which could be connected to a three-phase motor.

The switches must be controlled so that at no time are both switches in the same leg turned on or else the DC supply would be shorted. This requirement may be met by the complementary operation of the switches within a leg. i.e. if A^+ is on then A^- is off and vice versa. This leads to eight possible switching vectors for the inverter, V_0 through V_7 with six active switching vectors and two zero vectors.

Vector	A^+	B^+	C^+	A^-	B^-	C^-	V_{AB}	V_{BC}	V_{CA}	
V_0 = {000}	OFF	OFF	OFF	ON	ON	ON	0	0	0	zero vector
V_1 = {100}	ON	OFF	OFF	OFF	ON	ON	$+V_{dc}$	0	$-V_{dc}$	active vector
V_2 = {110}	ON	ON	OFF	OFF	OFF	ON	0	$+V_{dc}$	$-V_{dc}$	active vector
V_3 = {010}	OFF	ON	OFF	ON	OFF	ON	$-V_{dc}$	$+V_{dc}$	0	active vector
V_4 = {011}	OFF	ON	ON	ON	OFF	OFF	$-V_{dc}$	0	$+V_{dc}$	active vector
V_5 = {001}	OFF	OFF	ON	ON	ON	OFF	0	$-V_{dc}$	$+V_{dc}$	active vector
V_6 = {101}	ON	OFF	ON	OFF	ON	OFF	$+V_{dc}$	$-V_{dc}$	0	active vector
V_7 = {111}	ON	ON	ON	OFF	OFF	OFF	0	0	0	zero vector

Note that looking down the columns for the active switching vectors V_{1-6}, the output voltages vary as a pulsed sinusoid, with each leg offset by 120 degrees of phase angle.

To implement space vector modulation, a reference signal V_{ref} is sampled with a frequency f_s ($T_s = 1/f_s$). The reference signal may be generated from three

separate phase references using the transform. The reference vector is then synthesized using a combination of the two adjacent active switching vectors and one or both of the zero vectors. Various strategies of selecting the order of the vectors and which zero vector(s) to use exist. Strategy selection will affect the harmonic content and the switching losses.

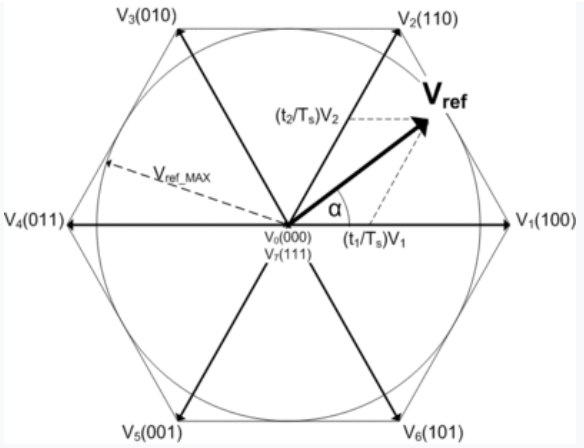

All eight possible switching vectors for a three-leg inverter using space vector modulation. An example V_{ref} is shown in the first sector. V_{ref_MAX} is the maximum amplitude of V_{ref} before non-linear over modulation is reached.

More complicated SVM strategies for the unbalanced operation of four-leg three-phase inverters do exist.

.

III.PROJECT DISCRIPTION AND CONTROL DESIGN

MATHEMATICAL MODEL OF THE TPFS INVERTER-FED PMSM DRIVE

Fig. 1 shows the topology of the TPFS inverter-fed PMSM drive. C1 and C2 denote the DC split capacitors, which are assumed to be identical (C1=C2=C). Considering cost reduction, the semiconductor switches of phase a are omitted. Instead, the stator of phase a is connected to the neutral point of the DC capacitors to provide an available approach for the stator current isa. Ls and Rs denote the stator resistance and inductance, respectively

The machine equations of a PMSM can be expressed as

$$\boldsymbol{u}_s = R_s \boldsymbol{i}_s + L_s \frac{d\boldsymbol{i}_s}{dt} + \boldsymbol{E} = R_s \boldsymbol{i}_s + \frac{d\boldsymbol{\lambda}_s}{dt} \qquad (1)$$

where us=[uan, ubn, ucn] T is the stator voltage vector, is=[isa, isb, isc] T is the stator current vector, E=[ea, eb, ec] T is the back-EMF of the PMSM, and λs is the stator linkage flux. Then, the stator flux equation can be expressed as

$$\boldsymbol{\lambda}_s = L_s \boldsymbol{i}_s + \boldsymbol{\lambda}_f \qquad (2)$$

where λf is the rotor flux. The electromagnetic torque of the PMSM can be expressed as

$$T_e = \frac{3}{2} p_n \boldsymbol{\lambda}_s \times \boldsymbol{i}_s = \frac{3}{2} p_n \left(L \boldsymbol{i}_s + \boldsymbol{\lambda}_f \right) \times \boldsymbol{i}_s = \frac{3}{2} p_n \boldsymbol{\lambda}_f \times \boldsymbol{i}_s \quad (3)$$

where pn is the number of pole pairs. The most commonly used control strategy for the PMSM is the so-called maximum torque per ampere (MTPA) because the stator current can be fully exploited to obtain the maximum possible torque. Based on the MTPA, the electromagnetic torque in the synchronized rotating frame is expressed as

$$T_e = \frac{3}{2} p_n [\lambda_f i_q + (L_d - L_q) i_d i_q] \quad (4)$$

In the surface-mounted PMSM case, the d- and q-axis inductances are equal to the synchronous inductance (Ld=Lq=Ls); thus, (4) can be simplified as

$$T_e = \frac{3}{2} p_n \lambda_f i_q \quad (5)$$

Therefore, using the magnitude of λs, (5) can be further expressed as

$$T_e = \frac{3}{2} p_n \lambda_f \frac{\lambda_{sq}}{L_q} = \frac{3}{2} p_n \lambda_f \frac{|\boldsymbol{\lambda}_s|}{L_s} \sin\delta \quad (6)$$

where δ is the angle between λs and λf. Neglecting Rs, us and is lag behind λs and λf by 90o , respectively; thus, δ is also the angle between us and is. To apply the MTPA, the magnitude of the stator flux and stator voltage at steady state can be expressed as follows:

$$|\boldsymbol{\lambda}_s| = \sqrt{\lambda_f^2 + \left(L_s T_e / 1.5 p_n \lambda_f \right)^2} \quad (7)$$

$$|\boldsymbol{u}_s| = \omega_r |\boldsymbol{\lambda}_s| = \omega_r \sqrt{\lambda_f^2 + \left(L_s T_e / 1.5 p_n \lambda_f \right)^2} \quad (8)$$

Thus, δ is expressed as

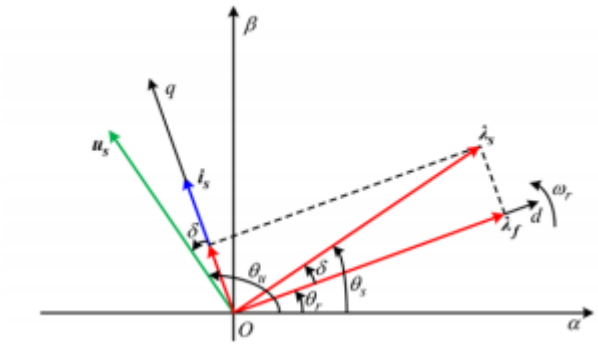

Fig. 3. Vector diagram of the PMSM under MTPA control.

$$\delta = \arccos \frac{\lambda_f}{|\boldsymbol{\lambda}_s|} = \arccos \frac{\lambda_f}{\sqrt{\lambda_f^2 + \left(L_s T_e / 1.5 p_n \lambda_f \right)^2}} \quad (9)$$

Based on (1)-(9), the vectors of the PMSM under the MTPA method are shown in Fig. 2. The rotational speed of the rotor flux and the synchronized rotating d-q coordinates is denoted by ωr, and θr=ωrt indicates the positions of the rotor flux. The positions of the stator flux and stator voltage are given by θs=θr+δ and θu=θr+δ+π/2, respectively

The key feature of the TPFS inverter-fed PMSM drive is its unique set of stator voltage vectors, which is completely different from that of a TPSS inverter. The stator voltage of the TPFS inverter-fed PMSM drive is given by

$$\boldsymbol{u}_s = \begin{bmatrix} u_a \\ u_b \\ u_c \end{bmatrix} = \frac{V_{DC1}}{6} \begin{bmatrix} -p_b - p_c - 2 \\ 2p_b - p_c + 1 \\ -p_b + 2p_c + 1 \end{bmatrix} + \frac{V_{DC2}}{6} \begin{bmatrix} -p_b - p_c + 2 \\ 2p_b - p_c - 1 \\ -p_b + 2p_c - 1 \end{bmatrix} \quad (10)$$

where pb and pc are switching functions defined as

$$p_j = \begin{cases} 1, S_j \, closed \\ -1, \overline{S_j} \, closed \end{cases} \quad j = b, c \quad (11)$$

representing the switching states of the four switches. Performing Clark's transformation and setting all possible combinations of the switching state to (10), the four basic vectors of the stator voltage in the α-β coordinate system are given in Table I

As seen from Table I, the zero vector, which fills in the remaining time portions aside from the active vectors in the SVM schemes, is absent in the TPFS inverters. Therefore, the equivalent zero vectors are synthesized using a pair of opposite vectors, therein producing additional complexity of the modulation strategies. Moreover, because the stator current isa flows directly into the neutral point of the DC bank, the node current equation of the neutral point can be expressed as

$$C \frac{dV_{DC1}}{dt} - C \frac{dV_{DC2}}{dt} = i_{sa} \quad (12)$$

According to Fig. 2, it is assumed that isa=|is|cos(ωrt+π/2). By integrating both sides of (12), the capacitor voltages at steady state are given by

$$V_{DC1} - V_{DC2} = \frac{|\boldsymbol{i}_s|}{\omega_r C} \cos(\omega_r t) \quad (13)$$

where the stator current magnitude |is|=iq=Te/1.5pnλf , and the capacitor voltage offset is assumed to be

ISSN(Online):2533-8945
VOLUME 4 ISSUE 4

zero. From (13), it is concluded that the capacitor voltages VDC1 and VDC2 are not

TABLE I
BASIC SPACE VECTORS OF THE TPFS INVERTER-FED PMSM DRIVE

Switching state (p_b, p_c)	u_α	u_β
U_1(0,0)	$2V_{DC2}/3$	0
U_2(1,0)	$(V_{DC2}-V_{DC1})/3$	$(V_{DC1}+V_{DC2})/\sqrt{3}$
U_3(1,1)	$-2V_{DC1}/3$	0
U_4(0,1)	$(V_{DC2}-V_{DC1})/3$	$-(V_{DC1}+V_{DC2})/\sqrt{3}$

constant in the TPFS inverter-fed PMSM drive; rather, they exhibit periodical fluctuations. Consequently, vectors of the TPFS inverter-fed PMSM drive are not symmetrical as in the TPSS inverters, which results in another challenge to the modulation strategy.

IV. ELIMINATION OF TORQUE RIPPLES CAUSED BY CAPACITOR VOLTAGE FLUCTUATIONS

In [1]-[11], the capacitor voltage fluctuations were not considered in the conventional modulation strategy; in other words, the effects of the capacitor voltage fluctuations on the electromagnetic torque were not exposed. A unified expression of the average switching functions was developed for the TPFS inverter-fed PMSM drive in [5], which is depicted by

$$\begin{bmatrix}\overline{p_b}\\ \overline{p_c}\end{bmatrix}=\frac{2\sqrt{3}|\boldsymbol{u}_s|}{V_{DC}}\begin{bmatrix}\sin(\omega_r t+\delta+\pi/6)\\ \sin(\omega_r t+\delta-\pi/6)\end{bmatrix} \quad (14)$$

can be considered as the $\begin{bmatrix}\overline{p_b} & \overline{p_c}\end{bmatrix}^T=\begin{bmatrix}2D_b-1 & 2D_c-1\end{bmatrix}^T$ where average values of pb and pc per switching period, in which Db and Dc are the duty ratios of the TPFS inverter-fed PMSM drive. However, the basic voltage vectors of the TPFS inverter are not symmetrical due to the capacitor voltage fluctuations, as shown in Table I. As shown in (14), the capacitor voltage fluctuations are not considered in the switching functions, resulting in deviations between the referenced and actual values of the stator voltages. Substituting (14) into (10) and applying Clarke's transformation, the stator voltage in the αβ coordinates can be expressed as

$$\begin{aligned}\begin{bmatrix}u_{s\alpha}\\ u_{s\beta}\end{bmatrix}&=|\boldsymbol{u}_s|\begin{bmatrix}-\sin(\omega_r t+\delta)\\ \cos(\omega_r t+\delta)\end{bmatrix}-\frac{1}{3}\begin{bmatrix}V_{DC1}-V_{DC2}\\ 0\end{bmatrix}\\ &=|\boldsymbol{u}_s|\begin{bmatrix}-\sin(\omega_r t+\delta)\\ \cos(\omega_r t+\delta)\end{bmatrix}-\frac{1}{3}\begin{bmatrix}|\boldsymbol{i}_s|\cos(\omega_r t)/\omega_r C\\ 0\end{bmatrix}\end{aligned} \quad (15)$$

It is worth nothing that the second item on the right side of (15) is generated by the conventional modulation method in addition to the expected first item. In other words, the stator voltages of the PMSM are unbalanced when utilizing the conventional method. As described in (1), the unbalanced stator voltages produce unbalanced stator currents if the stator impedance and the back-EMF are balanced. Therefore, the torque generated by the unbalanced stator current is distorted by low frequency harmonics, which are undesirable in the PMSM drive. To fully investigate the effect of the conventional method, the torque of the PMSM at steady state can be obtained by substituting (15) into (3):

$$T_e=\frac{3}{2}\cdot\frac{p_n|\boldsymbol{u}_s|\lambda_f}{\omega_r L_s}\left(\sin\delta-\int\frac{V_{DC1}-V_{DC2}}{3}dt\cdot\sin\omega_r t\right) \quad (16)$$

Substituting (13) into (16), the torque of the PMSM without

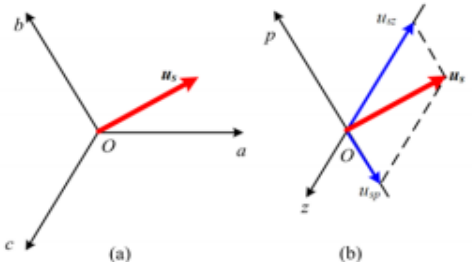

Fig. 4. Voltage vector in the (a) a-b-c frame; (b) proposed non-orthogonal stationary frame

$$T_e=\frac{3}{2}\cdot\frac{p_n|\boldsymbol{u}_s|\lambda_f}{\omega_r L_s}\left(\sin\delta-\frac{|\boldsymbol{i}_s|\cos 2\omega_r t}{6\omega_r^2 C}\right) \quad (17)$$

From (17), it is clear that there are 2nd-order harmonic components in the PMSM torque, which shows that the capacitor voltage fluctuations cannot be ignored in the PWM strategies for TPFS inverter-fed PMSM drives. Additionally, it is worth noting that the 2nd-order torque ripples increase under lower rotational speeds ωr. Consequently, if a proper compensation method is not applied, the 2nd-order torque ripples can be relatively large and thus deteriorate the stable operation of the PMSM drive at low speed. To reject the 2nd-order torque ripples, a

compensated PWM strategy considering capacitor voltage fluctuations should be provided. However, due to the capacitor voltage fluctuations and absence of the zero vectors, the modulation strategy for the TPFS inverter-fed PMSM drive becomes more sophisticated than that for a TPSS inverter. Consequently, complex computations involving trigonometric functions and irrational numbers were required during sector judgment and basic vector duration time calculations in previous studies [1]-[7]. Therefore, to avoid the overflow of a control period due to the complicated modulation scheme, the compensated modulation strategy should be simplified.

As shown in Fig. 3(a), a rotating voltage vector in the stationary a-b-c frame can be described as

$$\begin{aligned}\boldsymbol{u}_s &= \frac{2}{3}[u_{sa}+u_{sb}\cdot e^{j(2\pi/3)}+u_{sc}\cdot e^{j(4\pi/3)}]\\ &= \frac{2}{3}[(u_{sa}-u_{sa})+(u_{sb}-u_{sa})\cdot e^{j(2\pi/3)}+(u_{sc}-u_{sa})\cdot e^{j(4\pi/3)}]\\ &= \frac{2}{3}[u_{sp}\cdot e^{j(2\pi/3)}+u_{sz}\cdot e^{j(4\pi/3)}]\end{aligned} \quad (18)$$

where usp=usb-usa, and usz=usc-usa. According to (18), the voltage vector can be described by the new non-orthogonal p-z coordinates, as shown in Fig. 3(b). From (18), the coordinate transformation matrix is easily obtained as

$$T=\begin{bmatrix}-1 & 1 & 0\\ -1 & 0 & 1\end{bmatrix} \quad (19)$$

By introducing (19) into (10), the stator voltage of the TPFS inverter-fed PMSM drive is given by

$$\begin{bmatrix}u_{sp}\\ u_{sz}\end{bmatrix}=\frac{V_{DC}}{2}\begin{bmatrix}p_b\\ p_c\end{bmatrix}-\frac{1}{2}\begin{bmatrix}V_{DC1}-V_{DC2}\\ V_{DC1}-V_{DC2}\end{bmatrix} \quad (20)$$

According to (20), the average switching functions with the proposed modulation method can be expressed as

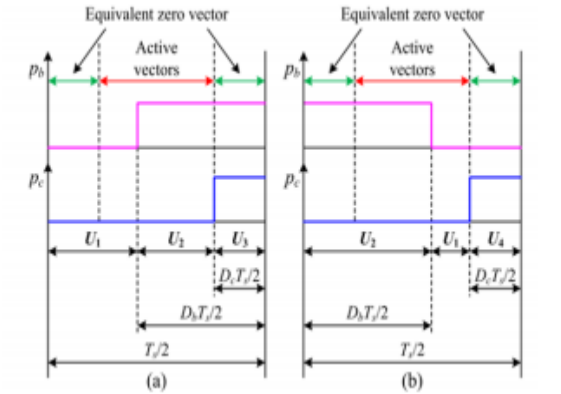

Fig. 5. Two alternative switching sequences for the TPFS inverter-fed PMSM drive: (a) using U1-U3 as the equivalent zero vector; (b) using U2-U4 as the equivalent zero vector.

$$\begin{aligned}\begin{bmatrix}\overline{p_b}\\ \overline{p_c}\end{bmatrix} &= \frac{2}{V_{DC}}\begin{bmatrix}u_{sp}\\ u_{sz}\end{bmatrix}-\frac{1}{V_{DC}}\begin{bmatrix}V_{DC1}-V_{DC2}\\ V_{DC1}-V_{DC2}\end{bmatrix}\\ &= \frac{2}{V_{DC}}\begin{bmatrix}u_{sb}-u_{sa}\\ u_{sc}-u_{sa}\end{bmatrix}-\frac{1}{V_{DC}}\begin{bmatrix}V_{DC1}-V_{DC2}\\ V_{DC1}-V_{DC2}\end{bmatrix}\\ &= \frac{2|\boldsymbol{u}_s|}{V_{DC}}\begin{bmatrix}\sin(\omega_r t+\delta+\pi/3)+\sin(\omega_r t+\delta)\\ \sin(\omega_r t+\delta-\pi/3)+\sin(\omega_r t+\delta)\end{bmatrix}-\frac{1}{V_{DC}}\begin{bmatrix}V_{DC1}-V_{DC2}\\ V_{DC1}-V_{DC2}\end{bmatrix}\\ &= \frac{2\sqrt{3}|\boldsymbol{u}_s|}{V_{DC}}\begin{bmatrix}\sin(\omega_r t+\delta+\pi/6)\\ \sin(\omega_r t+\delta-\pi/6)\end{bmatrix}-\frac{1}{V_{DC}}\begin{bmatrix}V_{DC1}-V_{DC2}\\ V_{DC1}-V_{DC2}\end{bmatrix}\end{aligned} \quad (21)$$

The switching functions in (21) are derived directly from the mathematical model of the TPFS inverter in the proposed p-z coordinate system, in which the effect of the capacitor voltage fluctuations is taken into account. Compared to the switching functions in (15), there is an additional item on the right side of (21), which can be taken as the compensated item for the capacitor voltage fluctuations. Considering the relationship between the average switching model and the duty ratios, the duty ratios of the TPFS inverter-fed PMSM drive can be directly calculated by

$$\begin{bmatrix}D_b\\ D_c\end{bmatrix}=\frac{1}{V_{DC}}\begin{bmatrix}u_{sp}+V_{DC2}\\ u_{sz}+V_{DC2}\end{bmatrix}=\frac{1}{V_{DC}}\begin{bmatrix}u_{sb}-u_{sa}+V_{DC2}\\ u_{sc}-u_{sa}+V_{DC2}\end{bmatrix} \quad (22)$$

To clarify the torque ripple rejection performance of the proposed compensated method, the torque of the PMSM is recalculated with the compensated duty ratios by introducing (21) into (11) (13) and (16), which is expressed as

$$T_e=\frac{3}{2}\cdot\frac{p_n|\boldsymbol{u}_s|\lambda_f\sin\delta}{\omega_r L_s} \quad (23)$$

It is concluded from (23) that the proposed compensated method fully rejects the 2nd-order torque ripples caused by the capacitor voltage fluctuations. Moreover, (22) also demonstrates great simplicity of the proposed method in that only simple calculations are required to directly obtain the duty ratios per switching period; the complex trigonometric calculations for sector judgment and vector duration time acquisition in [1]-[7] are avoided.

Once the duty ratios are determined, the next consideration is the switching sequence in the modulation strategies. Based on the different

ISSN(Online):2533-8945
VOLUME 4 ISSUE 4

approaches for zero vector synthesis, two alternative switching sequences are obtained. In [4] and [7], the

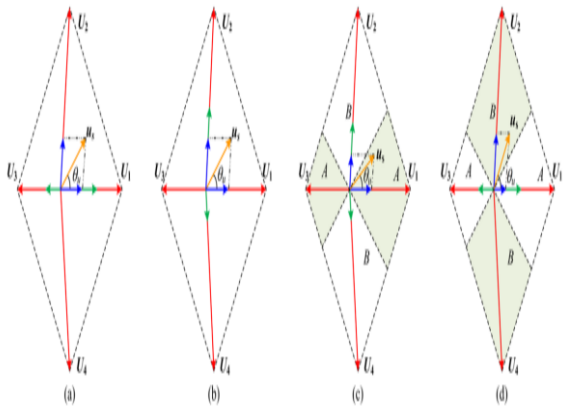

Fig. 6. SVM schemes for the TPFS inverter-fed PMSM drive: (a) SVSVM; (b) LVSVM; (c) NVSVM in Sector A; (d) NVSVM in Sector B.

zero vector is synthesized by the short pair of basic vectors U1-U3, leading to a unique SVM strategy—SVSVM, as shown in Fig. 4(a). Alternatively, in [6], the zero vector is synthesized by the long pair of basic vectors U2-U4, leading to another unique SVM strategy—LVSVM, as shown in Fig. 4(b). In addition, a special SVM strategy named NVSVM that synthesizes the reference voltage vectors by utilizing the nearest three basic vectors is proposed in [3] and [5]; specifically, the zero vector is synthesized by U1-U3 or U2-U4 alternatively during a fundamental period in NVSVM. The three vector synthesis approaches are presented in Fig. 5, where Sector A denotes $\theta u \in [-\pi/4, \pi/4] \cup [3\pi/4, 5\pi/4]$, and Sector B denotes $\theta u \in [\pi/4, 3\pi/4] \cup [5\pi/4, 7\pi/4]$.

It should be noted that the three SVM strategies only differs in their switching sequences; their duty ratios per switching period are identical, regardless of the zero vector synthesis method. Based on (22), all three SVM strategies are able to eliminate the 2nd-order torque ripples caused by the capacitor voltage fluctuations. However, the various switching sequences provide different stator voltage harmonic contents, leading to completely different torque harmonics, which are thoroughly analyzed in the next section.

V. EVALUATION OF SVM STRATEGIES FOR HIGH FREQUENCY TORQUE RIPPLE MINIMIZATION

As described above, three SVM strategies for the TPFS inverter-fed PMSM drive are developed according to their different zero vector synthesis methods, namely, SVSVM, LVSVM and NVSVM. Based on the different SVM strategies, the stator voltages are not purely sinusoidal; they contain various high-frequency harmonics contents, resulting in different torque harmonics in the PMSM. Hence, the SVM strategies for the TPFS inverter-fed PMSM drive should be evaluated to minimize high-frequency torque ripples. To investigate the relationship between torque ripples and the SVM strategies, the differential torque is deduced from (3)

$$\begin{aligned}\frac{dT_e}{dt} &= \frac{3p_n}{2}\left(\frac{d\boldsymbol{\lambda}_s}{dt}\times\boldsymbol{i}_s+\boldsymbol{\lambda}_s\times\frac{d\boldsymbol{i}_s}{dt}\right)\\ &= \frac{3p_n}{2}\left[(\boldsymbol{u}_s-R\boldsymbol{i}_s)\times\boldsymbol{i}_s+\frac{\boldsymbol{\lambda}_s}{L_s}\times\left(\boldsymbol{u}_s-R\boldsymbol{i}_s-\frac{d\boldsymbol{\lambda}_f}{dt}\right)\right]\end{aligned} \tag{24}$$

Neglecting stator resistance Rs, (24) is simplified as

$$\begin{aligned}\frac{dT_e}{dt} &= \frac{3p_n}{2}\left[\boldsymbol{u}_s\times\boldsymbol{i}_s+\frac{1}{L_s}(L_s\boldsymbol{i}_s+\boldsymbol{\lambda}_f)\times\left(\boldsymbol{u}_s-\frac{d\boldsymbol{\lambda}_f}{dt}\right)\right]\\ &= \frac{3p_n}{2L_s}\left(\boldsymbol{\lambda}_f\times\boldsymbol{u}_s-\boldsymbol{\lambda}_s\times\frac{d\boldsymbol{\lambda}_f}{dt}\right)\\ &= \frac{3p_n}{2L_s}\left(\boldsymbol{\lambda}_f\times\boldsymbol{u}_s-\int\boldsymbol{u}_s dt\times\frac{d\boldsymbol{\lambda}_f}{dt}\right)\end{aligned} \tag{25}$$

Because the rotor flux λf can be considered as constant within a small time period, the differentiated torque is further simplified as

$$\frac{dT_e}{dt}=\frac{3p_n}{2L_s}\cdot\boldsymbol{\lambda}_f\times\boldsymbol{u}_s \tag{26}$$

According to (26), the torque ripple caused by the switching operations is defined as

$$\begin{aligned}\overline{T}_e &= T_e-T_e^*\\ &= \frac{3p_n}{2L_s}\int\boldsymbol{\lambda}_f\times(\boldsymbol{u}_s-\boldsymbol{u}_s^*)dt\end{aligned} \tag{27}$$

where Te is the actual torque, Te * is the reference torque, us is the actual stator voltage vector, and us * is the reference stator voltage vector. From (27), it is clear that the stator voltage vector error (us-us *) is the main cause of the torque ripple in the TPFS inverter-fed PMSM drive. Fig. 6 shows the torque ripples produced by various SVM schemes under different utilization of vectors. To analytical evaluate the SVM strategies, the RMS value of the torque ripple proposed in [30], [31] is selected as the assessment criterion and defined as

$$\sigma=\sqrt{\frac{1}{T}\int_0^T\overline{T}_e^2\,dt} \tag{28}$$

Then, a case study on torque ripples using SVSVM is developed within a switching period when the symmetry is considered

$$\widetilde{T}_e=\begin{cases}\frac{3p_n}{2L_s}\left[\boldsymbol{\lambda}_f\times(\boldsymbol{U}_1-\boldsymbol{u}_s^*)\right]t, & 0<t<\frac{T_1}{2}\\ \frac{3p_n}{2L_s}\left\{\left[\boldsymbol{\lambda}_f\times(\boldsymbol{U}_2-\boldsymbol{u}_s^*)\right](t-\frac{T_1}{2})+\frac{\left[\boldsymbol{\lambda}_f\times(\boldsymbol{U}_1-\boldsymbol{u}_s^*)\right]T_1}{2}\right\}, & \frac{T_1}{2}<t<\frac{T_2}{2}\\ \frac{3p_n}{2L_s}\left[\boldsymbol{\lambda}_f\times(\boldsymbol{U}_3-\boldsymbol{u}_s^*)\right](t-\frac{T_s}{2}), & \frac{T_2}{2}<t<\frac{T_s}{2}\end{cases} \quad (29)$$

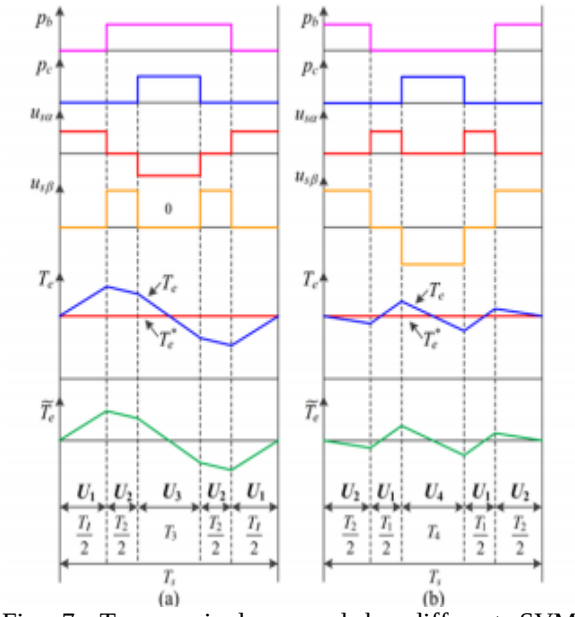

Fig. 7. Torque ripple caused by different SVM schemes: (a) SVSVM or NVSVM in Sector B; (b) LVSVM or NVSVM in Sector A.

TABLE II
PARAMETERS OF THE TPFS INVERTER-FED PMSM DRIVE

Parameter	Value
Pole pairs p_n	8
Stator resistance R_s	0.893 Ω
Stator inductance L_s	28.93 mH
Rotor flux λ_f	2.8047 V·s
DC capacitors C_1/C_2	2400 μF
Switching period T_s	1e-4 s

where T1, T2 and T3 are the duration times of active voltage vector U1, U2, and U3, which can be calculated as

$$\begin{cases}T_1=(1-D_b)T_s\\ T_2=(D_b-D_c)T_s\\ T_3=D_cT_s\end{cases} \quad (30)$$

According to (28), the torque ripple RMS value over a switching period can be calculated as:

$$\sigma_t=\sqrt{\frac{2}{T_s}\int_0^{T_s/2}\widetilde{T}_e^2dt} \quad (31)$$

Considering a complete fundamental cycle, the torque ripple RMS is calculated by substituting (31) into (28):

$$\sigma_T=\sqrt{\frac{1}{2\pi}\int_0^{2\pi}\sigma_t^2d\omega_1t}=\sqrt{\frac{1}{2\pi}\int_0^{2\pi}\left(\frac{2}{T_s}\int_0^{T_s/2}\widetilde{T}_e^2dt\right)d\omega_1t} \quad (32)$$

Combing (29), (30), and (32), the torque ripple RMS value over a fundamental cycle of SVSVM is obtained as

$$\sigma_{TSV}=\frac{\sqrt{30}p_n\lambda_fT_s}{240L_s}\left(5V_{DC}^2+\frac{810p_n^4\omega_m^4\lambda_f^4}{V_{DC}^2}-\frac{176\sqrt{3}p_n^3\omega_m^3\lambda_f^3}{\pi V_{DC}}-90p_n^2\omega_m^2\lambda_f^2\right)^{1/2} \quad (33)$$

where ωm=ωr/pn is the mechanical rotating speed of the PMSM. Similarly, the torque ripples caused by the LVSVM and NVSVM schemes are also obtained as

$$\sigma_{TLV}=\frac{\sqrt{10}p_n\lambda_fT_s}{80L_s}\left(5V_{DC}^2+\frac{270p_n^4\omega_m^4\lambda_f^4}{V_{DC}^2}-\frac{48p_n^3\omega_m^3\lambda_f^3}{\pi V_{DC}}-60p_n^2\omega_m^2\lambda_f^2\right)^{1/2} \quad (34)$$

$$\sigma_{TNV}=\frac{\sqrt{15}p_n\lambda_fT_s}{240L_s}\left[\left(10-\frac{20}{\pi}\right)V_{DC}^2+\frac{810p_n^4\omega_m^4\lambda_f^4}{V_{DC}^2}-\frac{\left(122\sqrt{6}+198\sqrt{2}\right)p_n^3\omega_m^3\lambda_f^3}{\pi V_{DC}}-\left(270-\frac{135}{\pi}\right)p_n^2\omega_m^2\lambda_f^2\right]^{1/2} \quad (35)$$

Based on (33)-(35), the torque ripple RMS values under the three SVM schemes are shown in Fig. 7. It is noted that the parameters used in (33)-(35) are listed in Table II and the DC voltage is equal to 500 V. It is concluded that LVSVM produces the largest torque ripple among the evaluated SVM schemes, which is undesirable in a TPFS inverter-fed PMSM drive. The SVSVM reduces the torque ripple by utilizing the short pair of vectors U1 and U3 to

ISSN(Online):2533-8945
VOLUME 4 ISSUE 4

synthesize the zero vectors. Because the stator voltage vector is synthesized by the three nearest vectors, the stator voltage vector error in the NVSVM is the smallest. Therefore, the NVSVM produces the minimum torque ripple, representing the favorable scheme for the proposed TPFS inverter-fed PMSM drive.

With the parameters of the proposed TPFS inverter-fed PMSM drive listed in Table II, the minimum required DC voltage VDCmin for linear modulation is depicted in Fig. 9 and Fig. 10. Clearly, the VDCmin calculated using (43) is related to

Fig. 11. Capacitor voltage offset suppression in the TPFS inverter-fed PMSM drive.

the electromagnetic torque Te, the capacitor voltage offset ΔVDC and the rotor speed ωm. In general, with increasing Te, the capacitor voltage fluctuation more severely deteriorates the linear modulation range, as seen from (38). Consequently, VDCmin increases with increasing Te, as shown in Fig. 9. Similarly, the capacitor voltage offset ΔVDC limits the full use of the DC bus voltage, which also deteriorates the linear modulation range of the TPFS inverter-fed PMSM drive. From Fig. 9 and Fig. 10, VDCmin increases linearly with increasing rotor speed ωm in the high rotor speed zone mainly because the stator voltage magnitude increases linearly with ωm, as depicted in (8). Nevertheless, when the rotational speed ωm is low, the capacitor voltage fluctuation is also aggravated, as seen from (38). Consequently, as shown in Fig. 9 and Fig. 10, a high value of VDCmin is required in the low rotational speed zone if taking capacitor voltage fluctuations into account, which is not seen in the conventional over-modulation judgment with (36). The proposed analysis provides sufficient insight into the linear modulation range of the TPFS inverter-fed PMSM drive, where the effects of the capacitor voltage fluctuations and offset are revealed. Therefore, the low frequency torque ripples caused by the over-modulation can be avoided by selecting an appropriate DC link voltage with (43).

As described above, the linear modulation range of the TPFS inverter-fed PMSM drive is deteriorated by the capacitor voltage offset. In practice, the dynamic behaviors of the PMSM, such as accelerating and decelerating, inject the DC component into the phase current, which produces the DC offset of the capacitor voltages. Thus, active control methods for suppressing the capacitor voltage offset are required to reduce torque ripples caused by the over-modulation. In [6] and [7], a close-loop control method in grid-connected applications is proposed for capacitor voltage offset suppression. The method utilizes a 2nd-order LPF to extract the DC component of the capacitor voltage offset and injects the compensated current component into the faulty phase, as shown in Fig

V.SIMULATION RESULTS

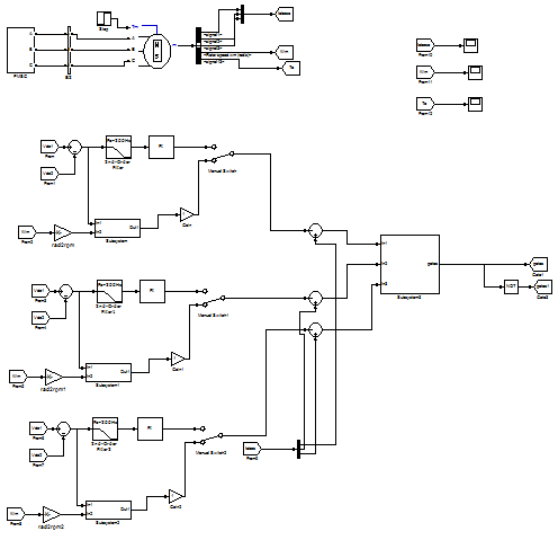

Fig: Proposed simulation diagram

ISSN(Online):2533-8945
VOLUME 4 ISSUE 4

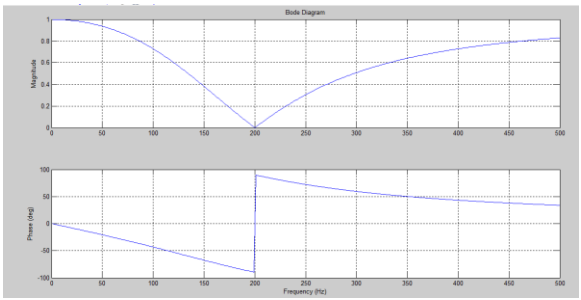

Fig: Bode plots

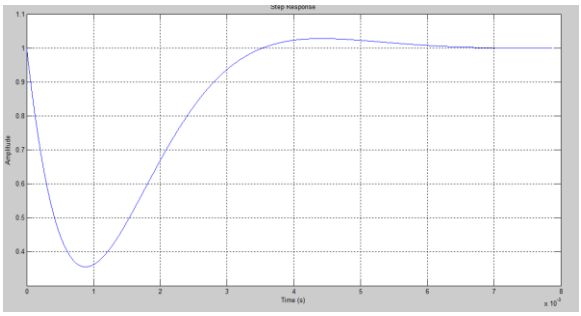

Fig: Step response

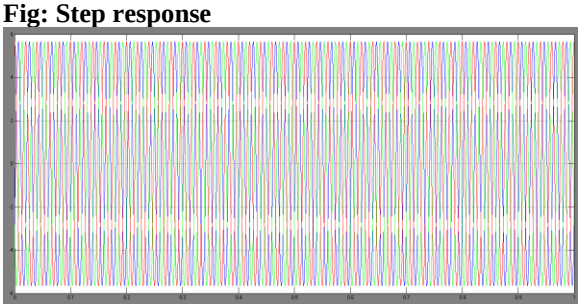

Fig:Stator currents

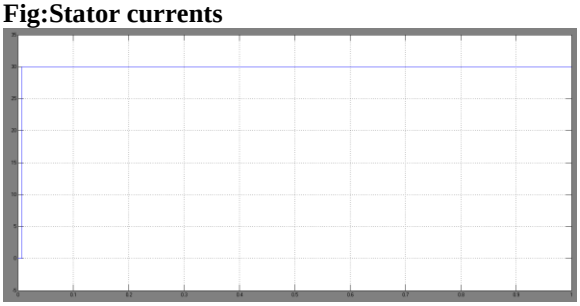

Fig: Speed

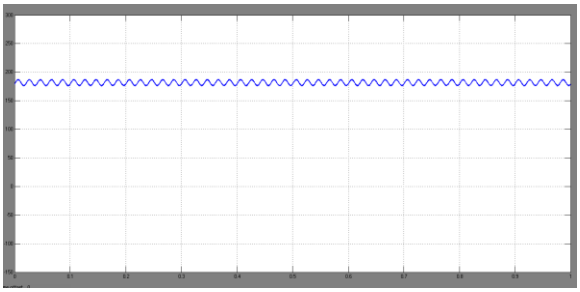

Fig: Torque

VI.CONCLUSION

This study gives sufficient insight into the causes and reduction of torque ripples in TPFS inverter-fed PMSM drives, and demonstrates that torque ripple reduction should be considered comprehensively from the perspective of capacitor voltage fluctuations, utilized SVM scheme, and linear modulation range.

A very simple compensated modulation method is proposed in this study to directly calculate the duty ratios by introducing a non-orthogonal coordinate transformation, which can eliminate the 2nd-order torque ripples caused by capacitor voltage fluctuations. For the high-frequency torque ripple reduction, three commonly used SVM schemes are evaluated based on the criterion of RMS torque ripple values. It is clear that using the NVSVM, which employs the three nearest vectors to synthesize the reference vector, is able to reduce the high torque ripple effectively in the TPFS inverter-fed PMSM drive. Moreover, to investigate the accurate linear modulation range of the TPFS inverter-fed PMSM drive, an in-depth analysis is proposed based on the duty ratio equations. The analysis exposes that the linear modulation range is strongly influenced by the torque, capacitor voltage offset and rotor speed. Then, the appropriate DC bus voltage can be chosen to avoid low-frequency torque ripples caused by over-modulation. In addition, an improved capacitor voltage offset suppression method is proposed by implementing an adaptive notch filter, which guarantees the sufficient stability margin of the control loop at low rotor speeds. The suppression method can eliminate the capacitor voltage offset, whereby the full exploitation of the DC bus voltage can be ensured.

REFERENCES

[1] H. W. Van der Broeck and J. D. Van Wyk, "A Comparative Investigation of a Three-Phase Induction Machine Drive with a Component Minimized Voltage-Fed Inverter under Different Control Options," IEEE Trans. Ind. Appl., vol. IA-20, no. 2, pp. 309-320, Mar. 1984.
[2] K. Gi-Taek and T. A. Lipo, "VSI-PWM rectifier/inverter system with a reduced switch count," IEEE Trans. Ind. Appl., vol. 32, no. 6, pp. 1331-1337, Nov./Dec. 1996.
[3] F. Blaabjerg, S. Freysson, H. H. Hansen, and S. Hansen, "A new optimized space-vector modulation strategy for a component-minimized voltage source inverter," IEEE Trans. Power Electron., vol. 12, no. 4, pp. 704-714, Jul. 1997.
[4] Z. Zeng, W. Zheng, R. Zhao, C. Zhu, and Q. Yuan, "Modeling, modulation, and control of the three-phase four-switch PWM rectifier under balanced voltage," IEEE Trans. Power Electron., vol. 31, no. 7, pp. 4892-4905, Jul. 2016.
[5] Z. Zeng, W. Zheng and R. Zhao, "Space-vector-based hybrid PWM strategy for reduced DC-link capacitor current stress in the post-fault grid-connected three-phase rectifier," IEEE Trans. Power Electron., vol. 63, no. 8, pp. 4989-5000, Aug. 2016.
[6] W. Wen, L. An, X. Xianyong, F. Lu, M. C. Thuyen, and L. Zhou, "Space vector pulse-width modulation algorithm and DC-side voltage control strategy of three-phase four-switch active power filters," IET Power Electron., vol. 6, no. 1, pp. 125-135, Jan. 2013.
[7] Z. Zeng, W. Zheng, R. Zhao, C. Zhu, and Q. Yuan, "The comprehensive design and optimization of the post-fault grid-connected three-phase PWM rectifier," IEEE Trans. Ind. Electron., vol. 63, no. 3, pp. 1629-1642, Mar. 2016.
[8] N. M. A. Freire and A. J. Marques Cardoso, "A Fault-Tolerant Direct Controlled PMSG Drive for Wind Energy Conversion Systems," IEEE Trans. Ind. Electron., vol. 61, no. 2, pp. 821-834, Feb. 2014.
[9] B. El Badsi, B. Bouzidi and A. Masmoudi, "DTC Scheme for a Four-Switch Inverter-Fed Induction Motor Emulating the Six-Switch Inverter Operation," IEEE Trans. Power Electron., vol. 28, no. 7, pp. 3528-3538, Jul. 2013.
[10]M. Masmoudi, B. El Badsi and A. Masmoudi, "DTC of B4-inverter-fed BLDC motor drives with reduced torque ripple during sector-to-sector commutations," IEEE Trans. Power Electron., vol. 29, no. 9, pp. 4855-4865, Sep. 2014